PHYSICAL REVIEW B **83**, 214113 (2011)

Roles of grain boundaries in improving fracture toughness of ultrafine-grained metals

T. Shimokawa,[1] M. Tanaka,[2] K. Kinoshita,[3] and K. Higashida[2]

[1]*School of Mechanical Engineering, College of Science and Engineering, Kanazawa University, Kakuma-machi, Kanazawa, Ishikawa 920-1192, Japan*

[2]*Department of Materials Science and Engineering, Kyushu University, 744 Motooka, Nishi-ku, Fukuoka 819-0395, Japan*

[3]*Division of Mechanical Science and Engineering, Graduate School of Natural Science and Technology, Kanazawa University, Kakuma-machi, Kanazawa, Ishikawa 920-1192, Japan*

(Received 13 December 2010; published 30 June 2011)

In order to improve the fracture toughness in ultrafine-grained metals, we investigate the interactions among crack tips, dislocations, and grain boundaries in aluminum bicrystal models containing a crack and $\langle 112\rangle$ tilt grain boundaries using molecular dynamics simulations. The results of previous computer simulations showed that grain refinement makes materials brittle if grain boundaries behave as obstacles to dislocation movement. However, it is actually well known that grain refinement increases fracture toughness of materials. Thus, the role of grain boundaries as dislocation sources should be essential to elucidate fracture phenomena in ultrafine-grained metals. A proposed mechanism to express the improved fracture toughness in ultrafine-grained metals is the disclination shielding effect on the crack tip mechanical field. Disclination shielding can be activated when two conditions are present. First, a transition of dislocation sources from crack tips to grain boundaries must occur. Second, the transformation of grain-boundary structure into a neighboring energetically stable boundary must occur as dislocations are emitted from the grain boundary. The disclination shielding effect becomes more pronounced as antishielding dislocations are continuously emitted from the grain boundary without dislocation emissions from crack tips, and then ultrafine-grained metals can sustain large plastic deformation without fracture with the drastic increase of the mobile dislocation density. Consequently, it can be expected that the disclination shielding effect can improve the fracture toughness in ultrafine-grained metals.

DOI: 10.1103/PhysRevB.83.214113 PACS number(s): 62.20.mt, 61.72.Mm, 61.72.Lk, 61.43.Bn

I. INTRODUCTION

The strength of crystalline metals is closely related to their internal structure. For example, for coarse-grained polycrystalline metals with a grain size larger than 1 μm, the yield strength increases as the grain size decreases. This phenomenon is known as the Hall-Petch relation,[1,2] where theoretically the main role of grain boundaries is to act as obstacles to dislocation movement. However, when the grain size decreases to less than one micrometer, grain size softening has been reported.[3–11] Because the volume fraction of the grain-boundary region cannot be neglected as the grain size decreases to 100 nm, grain-boundary-mediated plasticity, e.g., grain-boundary sliding and migration, might soften metals. These experimental results suggest that the main role of grain boundaries on the yield stress of crystalline metals changes according to the grain size.

In addition to the yield stress, fracture toughness has also been reported as being dependent on grain size for coarse-grained metals. Hodge *et al.* performed Charpy impact tests on coarse-grained metals at various temperatures. Their results show improved fracture toughness and a decrease of the ductile-brittle transition temperature (DBTT) with grain refinement.[12] It would be very interesting to investigate the dependence of fracture toughness on grain size in polycrystalline metals with even smaller grain size; however, until recently it was not easy to obtain metals with submicrometer grain size in bulk. Ultrafine-grained (UFG) metals with a grain size of the order of 100 nm can now be produced in bulk by severe plastic deformation;[13–15] hence we can now perform fracture tests with UFG metals. For UFG iron, improved fracture toughness at low temperatures as compared to coarse-grained iron has been reported,[16,17] and it has also been shown that the DBTT of UFG iron is lower than that of coarse-grained iron.[18]

A fundamental idea to explain the improved fracture toughness in single crystalline materials is dislocation shielding of the crack tip caused by the back stress created by dislocations emitted from the crack tip or dislocation sources around the crack tip.[19–21] In dislocation shielding theory, dislocation mobility significantly influences both fracture toughness and the DBTT.[22–24] In particular, it becomes hard for the dislocations emitted from the crack tip to glide away from the crack tip as the temperature decreases, and then it also becomes suppressed to emit additional dislocations from the crack tip because of the strong back stress on the crack tip. Finally, the material becomes brittle, indicating that it will fail in a brittle mode and no longer deform plastically.

In this paper, we investigate improving the fracture toughness of UFG metals. Because UFG metals contain a large number of grain boundaries, it can be easily supposed that the starting point of a fracture is not a singularity in intragranular regions but that in grain boundaries. However, detailed experimental analyses show that the activation energies estimated by the relationship between the DBTT and loading speed during four-point bending tests of UFG and coarse-grained iron are nearly the same, and the activation energy obtained is also very close to the activation energy for double kink nucleation along a screw dislocation in iron.[18] Therefore, the fracture toughness in polycrystalline metals with different grain sizes is also governed by dislocation mobility which does not show a grain size dependence. Based on dislocation shielding theory, in order to improve the fracture toughness with grain refinement, a stronger crack tip shielding effect is required without reducing the plastic deformation ability around the crack tip. The obvious difference between UFG and coarse-grained metals is the volume fraction of grain boundary regions. Thus, it is very important to investigate roles of grain boundaries for the plastic deformation by dislocations in satisfying the above necessary condition for improving the fracture toughness with grain refinement in polycrystalline metals.

The dependence of fracture toughness on grain size has been studied using molecular dynamics and discrete dislocation dynamics simulations.[26,27] In these models, grain boundaries are basically considered only as obstacles to dislocation motion. The results of these models show that fracture toughness decreases with grain refinement. However, this numerical result is contradicted by the experimental results that have been reported.[12,16,17] This shows that we cannot explain improved fracture toughness as shown in experiments if grain boundaries act as only obstacles to dislocation motion. On the other hand, there are numerous studies observing and describing dislocation emissions from grain boundaries in experiments[28,29] and atomic simulations;[30–34] thus we can expect that grain boundaries can act as a dislocation sources. Furthermore, it has been recently reported that a transformation of the grain-boundary structure with long periodicity into a neighboring favored boundary can occur by the emission of intrinsic grain-boundary dislocations from the grain boundary.[35]

It is difficult for conventional molecular dynamics simulations to describe the DBT phenomenon, which is driven by a delicate balance of thermally activated processes as mentioned previously, with the same time scale in the experiments, but molecular dynamics simulations have the advantage of providing detailed continuous atomic-scale information about defect interactions including grain boundaries that cannot be easily obtained by experimental work. We think the key factors to control the improving fracture toughness with grain refinement at low temperatures are not only the thermally activated process of the dislocation movement but also the role of grain boundaries as a dislocation source; therefore, in this paper, we use molecular dynamics simulations to investigate the effect of grain boundaries on the fracture toughness of UFG metals at low temperatures. In order to investigate roles of grain boundaries in improving fracture toughness, we perform the interaction simulations involving crack tips, dislocations, and grain boundaries in two aluminum bicrystal models containing grain boundaries with different dislocation source abilities under a condition close to the athermal process. Aluminum is a suitable model crystal for investigating defect interactions by using the results of atomic simulations compared with those of isotropic linear elastic theory because aluminum exhibits a nearly isotropic elastic property. Finally, based on the combined analyses of atomic simulations and linear elastic theory, we propose a mechanism to improve low-temperature fracture toughness considering grain boundary effects in UFG metals.

II. METHODOLOGY

Figure 1(a) shows a schematic of our aluminum bicrystal model that we use to investigate the influence of grain-boundary structures on the interaction among crack tips, dislocations, and grain boundaries. The embedded atom method proposed by Mishin *et al.* is adopted for simulating atomic interactions.[36] The bicrystal models consist of grains I and II, and grain I contains a crack with $L_c \approx 20$ nm at the center of the grain. Periodic boundary conditions are adopted in all directions. In order to make $\langle 112 \rangle$ tilt grain boundaries between these two grains, grains I and II are rotated through θ_I and θ_II about the $[\bar{1}\bar{1}2]$ tilt axis in clockwise and counterclockwise directions, respectively. Two models (A and B) containing different grain boundaries are prepared. Table I shows the detailed parameters for each model. In order to maintain the same value of Schmid factor of an active slip system for dislocations emitted from the crack tip in both models, we use a fixed θ_I for both models. For model A, the grain boundary takes a symmetrical $\Sigma 15$ structure by setting $\theta_\mathrm{II} = \theta_\mathrm{I}$. On the other hand, for model B, the grain boundary takes an asymmetrical structure by setting $\theta_\mathrm{II} = 17.67^\circ$; then the grain-boundary misorientation angle θ^B becomes 56.9°. The θ^B is very close to the symmetrical $\Sigma 105$ boundary with $\theta^{\Sigma 105} = 57.12^\circ$.[35] Furthermore, in order to investigate how the

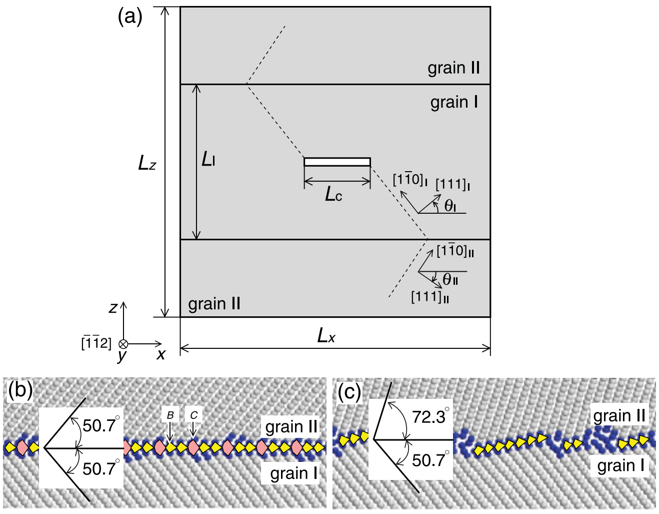

FIG. 1. (Color online) (a) Schematic of the bicrystal model containing a crack of physical length L_c. The interfaces are tilt grain boundaries with $\langle 112 \rangle$ tilt axis and the misorientation angle θ is the sum of θ_I and θ_II. (b) and (c) Symmetric $\Sigma 15$ expressed by the combination of B (yellow) and C (pink) structural units in model A and asymmetric $\Sigma 105$ grain-boundary structures expressed by the combination of B structural units and steps in model B, respectively. Here light and dark gray (blue) colored atoms indicate that their nearest neighbor atomic configurations correspond to an fcc structure and other defects defined using the common neighbor analysis,[25] respectively.

TABLE I. Parameters for bicrystal models containing symmetrical (S) and asymmetrical (A) tilt grain boundaries.

Model	θ_I	θ_II	GB Normals	GB Structure	Crack
A	39.23°	39.23°	$(5\bar{1}2)_\mathrm{I}//(1\bar{5}\bar{2})_\mathrm{II}$	$\Sigma 15$ S	Yes
A′	39.23°	39.23°	$(5\bar{1}2)_\mathrm{I}//(1\bar{5}\bar{2})_\mathrm{II}$	$\Sigma 15$ S	No
B	39.23°	17.67°	$(5\bar{1}2)_\mathrm{I}//(91,\overline{155},\overline{32})_\mathrm{II}$	$\Sigma 105$ A	Yes

crack tip influences the ability of the $\Sigma 15$ boundary to emit dislocations, we also prepare model A′ in which the crack tip is removed from grain I in model A.

Tensile tests along the z direction are performed for each model with a strain rate $\dot{\varepsilon}_z$ of 2×10^7 1/s. The analysis temperature is kept at $T = 100$ K using the velocity scaling method.[37] L_x is controlled to keep the nominal stress zero.[38] L_y is fixed during each analysis; thus, all tensile tests are performed under the plane strain condition.

Figures 1(b) and 1(c) show the symmetrical $\Sigma 15$ and asymmetrical $\Sigma 105$ grain-boundary structures in models A and B, respectively. The symmetrical $\Sigma 15$ boundary can be expressed by the combination of two structural units, B type and C type,[35] and the asymmetrical $\Sigma 105$ boundary can be expressed by a combination of B-type structural units and defect structures forming steps. The misorientation angle of $\Sigma 15$, $\theta^{\Sigma 15} = 78.46°$, is larger than that of $\Sigma 11$ showing a deep energy cusp, $\theta^{\Sigma 11} = 62.96°$, expressed by the single structural unit B. Therefore, when a tensile load is applied to the $\Sigma 15$ boundary along the normal direction of the plane, we observed that dislocations, whose line vectors are parallel to the tilt axis, are emitted from C-type structural units and that a transformation of the grain-boundary structure from $\Sigma 15$ to $\Sigma 11$ occurs.[35] On the other hand, we have also confirmed that the symmetrical $\Sigma 105$ boundary can emit dislocations, whose line vectors are parallel to the tilt axis, from A-type structural units under compressive loading, and then $\Sigma 105$ changes its structure to $\Sigma 11$. However, it is much harder for the symmetrical $\Sigma 105$ boundary to emit dislocations from the boundary under tensile loading than the $\Sigma 15$ boundary, and we observed that line vectors of these emitted dislocations are not parallel to the tilt axis.[35]

L_x, L_y, L_z, and L_{I} are set to be approximately 90 nm, 1.5 nm, 90 nm, and 45 nm, respectively, and periodic boundary conditions are used in all directions. When the line direction of an activating dislocation is not parallel to the tilt axis along the y direction, it is difficult to generate the dislocation from grain boundaries because of the geometrical constraint. Thus, it can be expected that the asymmetrical $\Sigma 105$ boundary in model B acts only as an obstacle to the dislocation motion under tensile deformation. On the other hand, it can be expected that the symmetrical $\Sigma 15$ boundary in model A acts not only as an obstacle to dislocation motion, but also as a dislocation source under tensile deformation. In this paper, we investigate the roles of grain boundaries in improving the fracture toughness in UFG metals by comparing the interactions among crack tips, dislocations, and grain boundaries observed in models A and B.

III. RESULTS

A. Transition of dislocation sources from crack tip to grain boundary

Figure 2(a) shows the relationship between the applied stress σ_{a} in the z direction and strain ε_z for each model. Black and white circles or squares represent dislocation emissions from the left crack tip and the upper-left grain boundary, respectively. For both models A and B, when grain I contains a crack, the first dislocation is generated from the left crack tip when σ_{a} reaches 1.34 GPa, and then σ_{a} decreases slightly; i.e., elastic strain energy is released by the dislocation emission. Three dislocations are emitted from the left crack tip in both models before the first dislocation emission from the grain boundary in model A, and it can be seen that the required stress to continue to generate following dislocations from the left crack tip becomes larger than the previous required stress for dislocation emission. These results show that the ability of the crack tip to generate dislocations becomes weaker because of the back stress of dislocations emitted from the crack tip. Note that when the second (or third) dislocation is emitted from the crack tip, the first (or second) dislocation emitted from the crack tip has already entered the grain boundary in both models. Thus, when the third dislocation is being emitted from the left crack tip, the upper-left grain boundary already contains two extra lattice dislocations. When tensile loading is further applied to both models after the third dislocation emission from the left crack tip, the stress-strain curves change dramatically because of the differences in the grain-boundary structures in each model.

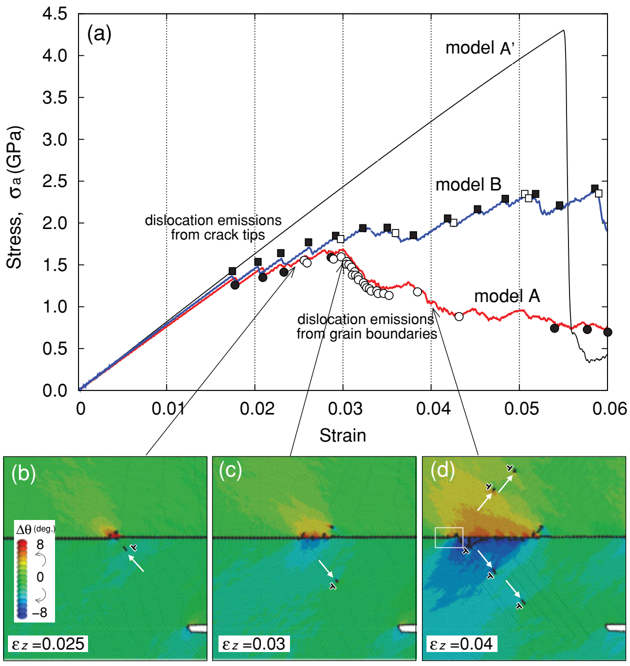

FIG. 2. (Color online) (a) Stress-strain curves of model A and model B containing a crack and model A′ with $\Sigma 15$ boundary without a crack. Black and white circles or squares represent dislocation emissions from the left crack tip and the upper-left grain boundary, respectively. 6 and 24 dislocations and 14 and 6 dislocations are emitted from the left crack tip and the upper-left grain boundary in model A and model B, respectively. (b)–(d) Translation of the dislocation source from the crack tip to the grain boundary in model A. Atomic color represents the rotation angle from the initial state of each atom taking the fcc structure, $\Delta\theta$. Black colored atoms represent defect structures. Detailed atomic structures in the white square in (d) are shown in Fig. 3.

1. *Results for model B*

Dislocation emissions from the left crack tip continue during tensile loading, and σ_{a} also continues to increase due to the back stress of dislocations emitted from the crack tip shown in Fig. 2(a). Although many dislocations impinge on the grain boundary or pile up against the grain boundary, it can be seen that few dislocations are still emitted from the grain boundary. This is due to the fact that the Schmid factor is small (only 0.29) for slip systems for dislocations along a line parallel to the tilt axis. In addition, the asymmetrical $\Sigma 105$ grain-boundary structure is expected to have only a limited ability to emit dislocations under tensile loading as mentioned in the previous section. Thus, when grain boundaries are functioning only as obstacles to dislocation motion, the applied stress σ_a continues to increase because of the strong shielding effect on the crack tip not to generate dislocations.

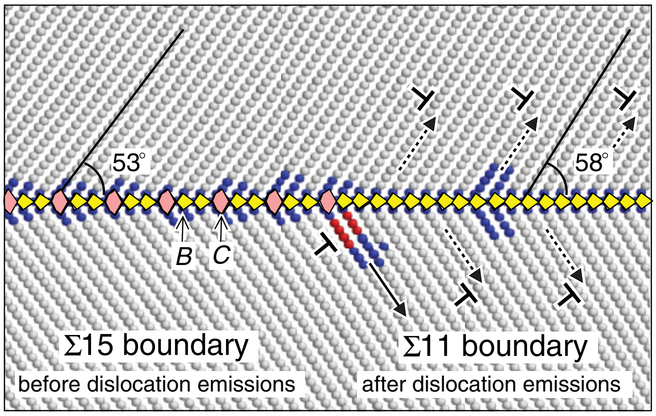

FIG. 3. (Color online) Change of grain-boundary structures from $\Sigma 15$ to $\Sigma 11$ after dislocation emissions from the *C* structural units (pink). This atomic structure corresponds to the enlarged picture in the white box shown in Fig. 2(d). Dark (red) and light gray (blue) colored atoms indicate that their nearest neighbor atomic configurations correspond to stacking fault structures and other defects, respectively. Atoms shown in other colors form an fcc structure.

2. Results for model A

Model A is expected to have grain boundaries that act as dislocation sources. As expected, numerous dislocations are emitted from the upper-left grain boundary after the third dislocation emission from the left crack tip shown in Fig. 2(a). Moreover, the crack tip does not emit any dislocations during dislocation emissions from grain boundaries (ε_z: 0.025$\sim$0.05), and therefore a transition of dislocation sources from the crack tip to the grain boundary occurs.[39] Atomic configurations when the transition occurs are shown in Figs. 2(b)–2(d). Atomic color represents the rotation angle from the initial state of each atomic configuration taking the fcc structure, $\Delta\theta$. $\Delta\theta$ is defined using the configurations of the first neighbors. Black colored atoms represent defect structures defined using common neighbor analysis.[25] Figure 2(b) shows the situation when the third dislocation emitted from the crack tip moves toward the grain boundary, and then dislocations are emitted from the grain boundary into grains I and II alternately as shown in Figs. 2(c) and 2(d). The enlarged picture in the white square in Fig. 2(d) is shown in Fig. 3. It can be seen that the $\Sigma 15$ grain-boundary structure transforms into the $\Sigma 11$ structure (expressed by only *B*-type structural units) because of dislocation emissions from the *C*-type structural units in the $\Sigma 15$ boundary. As shown in Fig. 2(d) and Fig. 3, the crystal orientation after dislocation motions rotates from the initial orientation, and it can be supposed that elastic fields corresponding to a disclination dipole[40] might occur after dislocation emissions from the grain boundary. As a result, σ_a suddenly decreases as the number of mobile dislocations increases because of dislocation emissions from grain boundaries.

From these atomic-scale computational experiments with models A and B, the influence of grain-boundary behavior can be clearly seen on the mechanical response of crystalline metals. Furthermore, it can be expected that the role of grain boundaries as either obstacles to dislocation motion or dislocation sources has an effect on the mechanical properties around the crack tip. In the following sections, we will investigate the role of grain boundaries on improving the fracture toughness of UFG metals on the basis of these atomic-scale computational experiments.

B. Grain-boundary shielding

The inset in Fig. 4 shows the resolved shear stress distribution $\tau_{z^I x^I}$ for the activated slip system of dislocations emitted from the left crack tip in model A. The local shear stress at a distance of 0.4 nm from the left crack tip is defined as τ_{ck}^{L}. Figure 4 shows the relationship between τ_{ck}^{L} and σ_a until ε_z reaches 0.025. We have confirmed the same relationship shown in Fig. 4 for the right crack tip. Before the first dislocation emission, the absolute value of τ_{ck}^{L} linearly increases with σ_a. When τ_{ck}^{L} reaches approximately -1.7 GPa, the first dislocation is emitted from the left crack tip. Although σ_a increases after the first dislocation emission, $|\tau_{ck}^{L}|$ cannot take larger stress values than the value of $|\tau_{ck}^{L}|$ required for the first dislocation emission. Therefore, the critical value of the local shear stress required for dislocation emissions from the crack tip is $\tau_{ck,c}^{L} \approx -1.7$ GPa. Because σ_a gradually increases to generate subsequent dislocations from the crack tip, the potential for plastic deformation around the crack tip

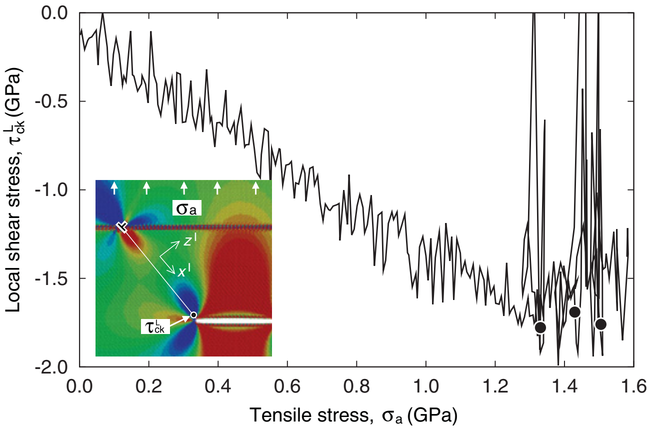

FIG. 4. (Color online) Relationship between the local resolved shear stress of the slip system τ_{ck}^{L} at a distance of 0.4 nm from the left crack tip and the tensile stress σ_a in model A until $\varepsilon_z = 0.025$. The inset figure shows the distribution of resolved shear stress of $\tau_{z^I x^I}$. Solid circles represent the required stress for dislocation emissions from the left crack tip.

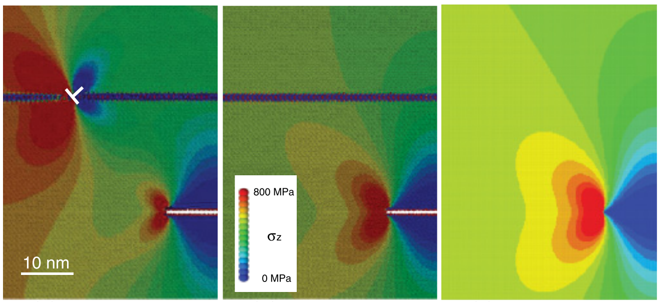

(a)$\sigma_a = 0.5$ GPa (b)$\sigma_a = 0.5$ GPa (c)$\sigma_A = 0.5$ GPa

FIG. 5. (Color online) Stress fields of σ_z around the left crack tip in model A at 0 K. (a) Grain-boundary shielding by the nonequilibrium grain boundary containing one EGBD. (b) Equilibrium grain boundary. (c) Theoretical stress field of a Griffith-Inglis crack under an applied stress σ_A according to linear elastic theory.

weakens because of the back stress of dislocations impinging on the grain boundary.

On the other hand, Figs. 5(a) and 5(b) shows the normal stress distributions σ_z around the left crack tip in model A with and without extrinsic grain-boundary dislocations (EGBDs) when $\sigma_a = 0.5$ GPa. We can clearly see that EGBDs can shield the mechanical fields around the crack tip. Hence, it can be expected that fracture toughness can be improved by the impinging dislocations at grain boundaries.

Generally, the effect of lattice dislocations on the mechanical field around the crack tip is called *dislocation shielding*, and the shielding effect significantly influences both dislocation emission and cleavage fracture phenomena around the crack tip. Furthermore, when grain boundaries exist around crack tips, impinging lattice dislocations at grain boundaries can also affect the mechanical properties of the crack tip as confirmed in Figs. 4 and 5, so the effect of EGBDs on the mechanical field around the crack tip can be called *grain-boundary shielding*.[17,18] Grain-boundary shielding naturally shows grain size dependence; thus this phenomenon is very important for our investigation into the effect of grain boundaries on fracture phenomenon in UFG metals. Therefore, in the remainder of this section we examine the validity of the grain-boundary shielding observed in the atomic simulations in comparison with the dislocation shielding predicted by linear elastic theory.

First, we estimate the effect of grain-boundary shielding using linear fracture mechanics. For the dislocation shielding shown in Fig. 6(a), the local stress intensity factor k around the crack tip can be calculated by considering lattice dislocations as follows:[41]

$$k = K + \sum_{i}^{n_{\text{dislo}}} k_{\text{dislo},i}. \tag{1}$$

Here, K and $k_{\text{dislo},i}$ are stress intensity factors caused by the applied stress and dislocations, respectively, and n_{dislo} is the number of dislocations affecting the crack tip mechanical fields. When dislocation i exists on an atomic plane inclined θ_i to the crack plane and takes a distance r_i from the crack tip, $k_{\text{dislo},i}$ can be estimated using linear elastic theory as follows:[19,42]

$$k_{\text{dislo},i} = -\frac{3\mu b_i}{2(1-\nu)\sqrt{2\pi r_i}} \cos\frac{\theta_i}{2} \sin\theta_i. \tag{2}$$

Here, μ, ν, and b_i represent the shear modulus, Poisson's ratio, and Burgers vector of dislocation i, respectively. Based on the dislocation shielding mentioned above and taking into account the grain-boundary shielding as shown in Fig. 6(b), the local stress intensity factor k can be expressed as

$$k = K + \sum_{i}^{n_{\text{dislo}}} k_{\text{dislo},i} + \sum_{i}^{n_{\text{gb}}} k_{\text{gb},i}. \tag{3}$$

Here, $k_{\text{gb},i}$ is the stress intensity factor caused by dislocation i at a grain boundary and n_{gb} is the number of dislocations at grain boundaries. When we suppose that the elastic field caused by dislocation i with b_i at a grain boundary shows the same elastic field caused by dislocations i with b_i at an intragranular region, $k_{\text{gb},i}$ can be easily regarded as $k'_{\text{gb},i} \equiv k_{\text{dislo},i}|_{r=r_{\text{gb},i}}$. Here, $r_{\text{gb},i}$ is the distance between the crack tip and dislocation i at the grain boundary shown in Fig. 6(b). Because Eq. (2) is available for an isotropic elastic body, the shear modulus μ and Poisson's ratio ν represented by the atomic potential expressing the anisotropic elastic body are estimated by the Voigt approximation,[43] and thereby we can obtain $\mu = 29.2$ GPa and $\nu = 0.33$. When we consider b^{lt} as the Burgers vector of lattice dislocation, the grain-boundary shielding effect caused by dislocation l_t with b^{lt} shown in

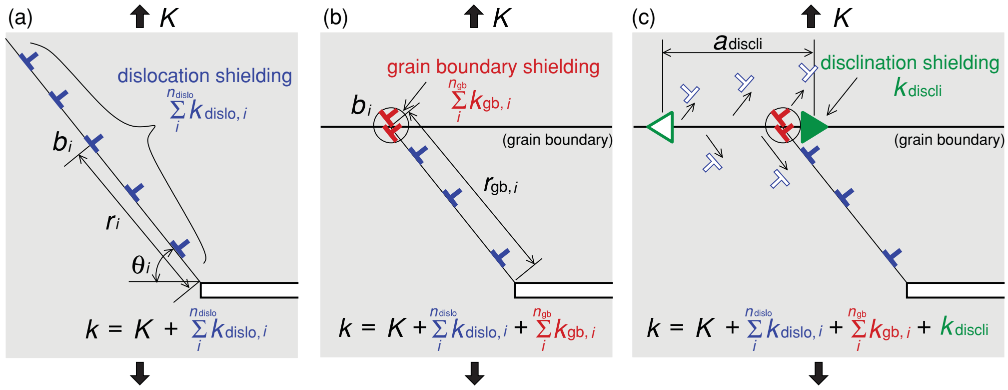

FIG. 6. (Color online) Schematic representations of (a) dislocation, (b) grain boundary, and (c) disclination shielding. K and k represent the apparent macroscopic and the actual local stress intensity factors, respectively. $k_{\text{dislo},i}$, k_{gb}, and k_{discli} also represent the stress intensity factor due to dislocation, grain boundary, and disclination shielding, respectively.

Fig. 5(a) can be estimated by $k'_{\mathrm{gb},l_t} = -0.031\ \mathrm{MPa}\sqrt{\mathrm{m}}$ using Eq. (2), based on linear elastic theory.

Next, the availability of k'_{gb,l_t} expressed by Eq. (2) is confirmed using the results of dislocation emissions from the crack tip in our atomic-scale computational experiments. The analysis model shown in Fig. 1(a) is applied to periodic boundary conditions in all directions, so the crack's periodicity array is in the x and z directions. In order to compare the crack tip stress field appearing in the atomic model and estimated by the linear elastic theory, Fig. 5(c) shows the Griffith-Inglis crack tip stress field of σ_z under an applied stress $\sigma_A = 0.5$ GPa.[44] A Griffith-Inglis crack can express the stress field at a distance r from the crack tip even though r is comparable to the crack length a. When a is much larger than r, the Griffith-Inglis crack tip stress field is comparable to the stress field expressed by the stress intensity factor K. Because the anisotropic factor calculated by $c_{44}/(c_{11} - c_{12})$ is 1.25 for aluminum (expressed by the atomic potential), the stress fields in the atomic model expressing the anisotropic elastic body and in the isotropic elastic body shown in Figs. 5(b) and 5(c) are in good agreement. Hence, we suppose that the mechanical field in the vicinity of the crack tip in the atomic model can be accurately modeled using the stress intensity factor K and linear elastic theory. The stress intensity factor K considering the correction factor for cracks arrayed in a row at regular intervals W can be obtained as follows:[45]

$$K = \sigma\sqrt{\pi a}\left(\frac{W}{\pi a}\tan\frac{\pi a}{W}\right). \tag{4}$$

Here, a and W are set to be $L_c/2$ and L_x, respectively.

Although dislocations are emitted from the crack tip in atomic simulations in this study, we suppose that dislocations are emitted from a dislocation source at r_s from the crack tip in order to evaluate k_{gb,l_t} using atomic simulations and linear elastic theory. Generally, a dislocation can be generated from the dislocation source when a force acting on the dislocation f_d follows the following relation:

$$f_d = f_{Kd} + f_{d^2} + f_{dd'} > f_f. \tag{5}$$

Here, the force direction keeping away from the crack tip is positive. f_{Kd}, f_{d^2}, and $f_{dd'}$ represent the direct crack-dislocation force, the self-image force, and the dislocation-dislocation interaction force, respectively.[41] When the resultant force f_d becomes larger than the friction force f_f, the dislocation at the dislocation source near the crack tip can be released. Because the atomic simulation shows a constant value of $\tau^{L}_{\mathrm{ck,c}} \approx -1.7$ GPa for the dislocation emission from the crack tip shown in Fig. 4, we can regard f_f as a constant in Eq. (5). For f_{d^2}, it does not depend on the applied stress and other dislocation positions; hence we can also regard f_{d^2} as a constant. Thus, we can suppose that the dislocation emission from the dislocation source near the crack tip occurs when the value of $f_{Kd} + f_{dd'}$ becomes larger than the constant value of $f_f - f_{d^2}$.

When we focus on the first and second dislocation emissions from the dislocation source near the crack tip, the following equation should hold according the former discussion:

$$f^1_{Kd} = f^2_{Kd} + f^2_{dd'}. \tag{6}$$

Here, the superscript represents the order of dislocations emitted from the dislocation source. When the first dislocation is emitted from the dislocation source, there is no dislocation around the dislocation source. Therefore, $f^1_{dd'}$ becomes zero. $f^2_{dd'}$ can be estimated by $-\mu b^2/2\pi(1-\nu)(r_{gb} - r_s)$ based on dislocation theory[46] when we suppose that the Burgers vector of impinging dislocations at the grain boundary does not change from that of the lattice dislocation. f_{Kd} can be calculated by the local stress intensity factor k in Eq. (3), and therefore, f^1_{Kd} and f^2_{Kd} can be evaluated by the crack tip stress fields expressed by the local stress intensity factors $k^1_e = K^1_e$ and $k^2_e = K^2_e + k_{\mathrm{gb},l_t}$, respectively. Here, K^j_e and k^j_e are the critical applied stress intensity factor and the critical local stress intensity factor required for the jth dislocation emission from the dislocation source. For model A in the atomic simulations, the first and second dislocations are emitted when σ_a reaches $\sigma^1_a = 1.34$ GPa and $\sigma^2_a = 1.47$ GPa, respectively; hence it can be estimated that $K^1_e = 0.248\ \mathrm{MPa}\sqrt{\mathrm{m}}$ and $K^2_e = 0.272\ \mathrm{MPa}\sqrt{\mathrm{m}}$ using Eq. (4), and then we can obtain $f^1_{Kd} = 0.48$ N/m. Because we can obtain all the values of the forces and the stress intensity factors, except for k_{gb,l_t}, in order to calculate Eq. (6), we can finally estimate $k_{\mathrm{gb},l_t} = -0.029\ \mathrm{MPa}\sqrt{\mathrm{m}}$ when $r_s = 0.4$ nm without Eq. (2). Because k'_{gb,l_t} estimated by Eq. (2) and k_{gb,l_t} estimated without Eq. (2) agree well, we consider that the impinging dislocation at the grain boundary maintains the same stress field as the lattice dislocation during the atomic simulation, although the dislocation core structure changes after the dislocation impinges on the grain boundary. In other words, the component of the Burgers vector of the impinging dislocation is conserved inside a local area in the vicinity of the impinged site of the grain boundary during the atomic simulation under a condition close to an athermal process. Generally, the impinging dislocations correspond to EGBDs and there is a possibility that EGBDs change their structures into IGBDs with no long-range stress field.[47] It is hard for molecular dynamics methods to reproduce the phenomena because of the treatable time-scale restriction. However, the accommodation process, controlled by grain-boundary diffusion, requires enough annealing time at high temperature and it has been observed in experiments that an EGBD in nickel changes its structure into a quasiperiodic network after annealing for several tens of minutes at over $0.3T_m$ where T_m is melting temperature.[48] Hence, it is reasonable to suppose that the stress field caused by impinging dislocations is maintained during fracture tests at low temperatures in experiments.[16,17] Consequently, the effect of grain-boundary shielding on the crack tip caused by dislocation i at a grain boundary, $k_{\mathrm{gb},i}$, can be estimated simply by using Eq. (2).

C. Effect of extrinsic grain-boundary dislocations (EGBDs) on fracture toughness

When grain boundaries exist around a crack tip and they act as obstacles against dislocation motion as well as a sink site for incoming dislocations, both dislocation and grain-boundary shielding effects occur as shown in Fig. 6(b). In this case, however, the back stress of these dislocations around the grain boundary is expected to make it more difficult to continue further dislocation emission from the crack tip as compared

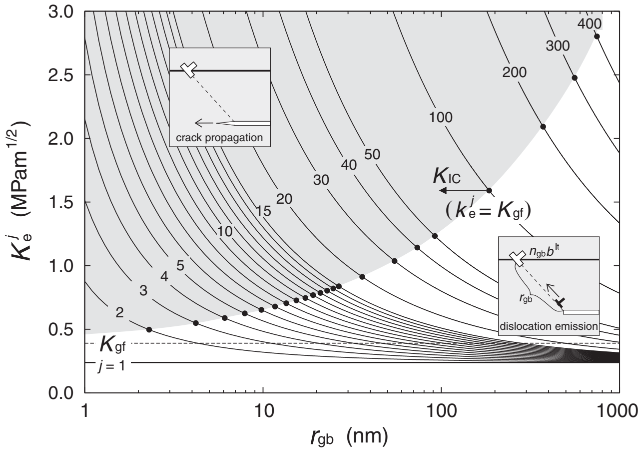

FIG. 7. The effect of back stress due to extrinsic grain-boundary dislocations on the applied stress intensity factor K_e^j required to emit the jth dislocation from the crack tip as a function of changes in the distance between the crack tip and EGBDs, r_{gb}. When the jth dislocation is emitted from the crack tip, the number of extrinsic grain-boundary dislocations n_{gb} is $j-1$. Solid circles represent the points at which the local k_e^j reaches the critical values of Griffith level, K_{gf}, namely the points where the crack propagates without dislocation emission. Thus, solid circles represent the fracture toughness K_{IC} for r_{gb}.

to when there are no grain boundaries around the crack tips, as shown in Fig. 6(a). Furthermore, the effect of back stress against the dislocation emission from the crack tip becomes more significant as r_{gb} decreases. In this section, we investigate the effect of grain-boundary shielding on the fracture toughness of polycrystalline materials.

In order to estimate fracture toughness, we first suppose a fracture condition for the crack tip in our atomic models, because the crack never showed cleavage during the atomic simulations in this study. fcc structures have scarcely been observed in conjunction with brittle fractures in coarse-grained metals. However, it has been recently reported that a purely brittle fracture mode in the absence of dislocations can occur under tensile loading for Cu nanowhiskers that are approximately 200 nm in diameter.[49] Therefore, for simplicity, we use the Griffith's criterion[50] with an assumption of a (111) cleavage plane. The atomic potential used in this study shows the (111) surface energy $\gamma_{(111)} = 870$ mJ/m^2, and then the Griffith's criterion K_{gf} can be estimated as 0.39 MPa$\sqrt{\text{m}}$: namely, the cleavage fracture mode will occur if k [as estimated by Eq. (3)] is larger than K_{gf}.

Figure 7 shows the relationship between r_{gb} and the applied stress intensity factor K_e^j required to emit the jth dislocation from the dislocation source near the crack tip, when only the grain-boundary shielding effect is considered. In this scenario, all dislocations emitted from the dislocation source near the crack tip impinge on the grain boundary without dislocation pileup against the grain boundary; i.e., all emitted dislocations form a super-dislocation with the resultant Burgers vector of these emitted dislocations at the grain boundary. The condition for the jth dislocation emission can be estimated as $f_{Kd}^j + f_{dd'}^j = f_{Kd}^1$. Because f_{Kd}^1 has already been determined in the previous section and $f_{dd'}^j$ can be calculated using dislocation theory, we can estimate the value of f_{Kd}^j required to emit the jth dislocation. The local intensity factor k_e^j can be calculated by f_{Kd}^j, and then K_e^j can be obtained using Eq. (3). Here, n_{gb} corresponds to $j-1$ and $k_{gb,j-1} = k_{gb,l_t}$ is estimated by Eq. (2). The black circles in Fig. 7 indicate the points where cleavage fracture begins at the crack tip, i.e., where the value of k_e^j reaches K_{gf}; hence, the black circles represent the fracture toughness K_{IC} for r_{gb}. For example, for $r_{gb} = 10$ nm, k_e^6 is equal to K_{gf}, so K_e^6 represents the fracture toughness K_{IC} for the material considering only the grain-boundary shielding effect.

Because r_{gb} represents the distance between the crack tip and EGBDs, we can use r_{gb} to estimate grain size. As shown in Fig. 7, since grain-boundary shielding does not occur for $j = 1$, we can see that K_e^1 does not show any dependence on grain size. When j is larger than 2, K_e^j show a dependence on grain size caused by grain-boundary shielding; K_e^j increases as the grain size decreases. It can also be seen that the K_{IC} values plotted in Fig. 7 are always larger than the K_{gf} broken line; thus fracture toughness is improved as a consequence of grain-boundary shielding. Note here that K_{IC} decreases with decreasing grain size. This is understood by the calculation result that the grain-boundary shielding effect only due to EGBDs is very limited because dislocation emission from the crack tip is hindered by the effect of back stress of EGBDs. The same dependence on grain size of K_{IC} has been reported using discrete dislocation dynamics simulations where grain boundaries are considered as only acting as obstacles to dislocation motion.[27] However, such results obtained by considering the effects of EGBDs cannot explain the results observed in actual experiments that show improved fracture toughness with grain refinement.[12,16–18] As a result, in order to understand the mechanism improving the fracture toughness with grain refinement, we need to consider another shielding effect to improve K before k reaches K_{gf}, in addition to the dislocation shielding effect $k_{dislo,i}$ and also to the grain-boundary shielding effect $k_{gb,i}$. In the following section, we investigate another shielding effect by paying attention to the function of grain boundaries as dislocation sources observed in atomic simulations of model A.

D. Dislocation emissions from grain boundaries

In models A and A′ with and without a crack, 1.5 GPa and 4.3 GPa are required to emit dislocations from the grain boundary shown in Fig. 2(a), respectively. This means that in our simulations, grain boundaries around the crack tip can emit dislocations 35% easier than grain boundaries not around the crack tip. In order to investigate the reason why the stresses required for dislocation emissions from grain boundaries are so different, we show atomic structures around the upper-left grain boundaries just before dislocation emission in Fig. 8. Note that the grain boundary shown in Fig. 8(a) already contains two lattice dislocations emitted from the crack tip and the third dislocation is coming into the grain boundary in model A. We also show the changes of local resolved shear stresses $\tau_{gb}^L (= \tau_{z^{II}x^{II}})$ with strain, and stress-strain curves for σ_a^A and $\sigma_a^{A'}$ in Fig. 8(c). Light gray (red) and dark gray (blue) lines represent local resolved shear stresses $\tau^{\mathrm{L},\alpha}_{\mathrm{gb}}$ and $\tau^{\mathrm{L},\beta}_{\mathrm{gb}}$ at the sight of α and β on slip planes of the first dislocations (D^{b}) from $\Sigma 15$ boundaries in models A and A′, respectively. Thick and thin black lines represent the tensile stresses σ_{a} in model A and model A′, respectively. Both $\tau^{\mathrm{L},\alpha}_{\mathrm{gb}}$ and $\tau^{\mathrm{L},\beta}_{\mathrm{gb}}$ increase linearly with nearly the same angle for $\sigma^{\mathrm{A}}_{\mathrm{a}}$ and $\sigma^{\mathrm{A}'}_{\mathrm{a}}$. Hence, in order to obtain a critical $\tau^{\mathrm{L},\beta}_{\mathrm{gb}}$ for the dislocation emission from the grain boundary in model A′ without any intragranular dislocation source, $\sigma^{\mathrm{A}'}_{\mathrm{a}}$ should take the larger value 4.3 GPa as a result. On the other hand, for model A, $\tau^{\mathrm{L},\alpha}_{\mathrm{gb}}$ dramatically increases when the first and second dislocations emitted from the crack tip impinge on the grain boundary, then dislocation D^{a} is first emitted from a *C*-type structural unit into grain II when the strain reaches 0.021. The Burgers circuit shown in Fig. 8(a) reveals that dislocation D^{a} has the Burgers vector of a perfect lattice dislocation, but the dislocation does not extend into Shockley partials. As a result, dislocation D^{a} remains near the grain boundary. We discuss an explanation for this in the next section. When the third dislocation is approaching the grain boundary, $\tau^{\mathrm{L},\alpha}_{\mathrm{gb}}$ increases further, then dislocation D^{b} is emitted from the neighboring *C*-type structural unit of dislocation D^{a}. Because dislocation D^{b} enters grain II and releases more stored elastic energy than dislocation D^{a}, we consider dislocation D^{b} as the real first dislocation emission from the grain boundary. The difference between the values of $\tau^{\mathrm{L}}_{\mathrm{gb}}$ required to emit a dislocation from the grain boundaries in models A and A′ might be due to the normal stress component's dependence on the critical $\tau^{\mathrm{L}}_{\mathrm{gb}}$ to emit a dislocation from the grain boundary.[34] Thus, model A can generate dislocations from the grain boundary easier than model A′, due to the stress concentration at the grain boundary caused by dislocations emitted from the intragranular dislocation source.

Based on the results obtained from our atomic-scale computational experiments, we can confirm the transition of dislocation sources from crack tips to grain boundaries. Crack tips show the first largest stress concentration source, so dislocations are emitted first from crack tips. However, grain-boundary shielding caused by these dislocations impinging on grain boundaries makes it difficult for crack tips to emit dislocations. On the other hand, local stress fields near grain boundaries are drastically increased by impinging dislocations at grain boundaries, and grain boundaries change their equilibrium structure into nonequilibrium grain-boundary structures. As a result, stress concentration fields first shift from crack tips to grain boundaries by dislocation pileup against grain boundaries and impinging dislocations at grain boundaries, and then nonequilibrium grain boundaries can generate dislocations at lower applied stresses than equilibrium grain boundaries. Consequently, the transition of dislocation sources from crack tips to grain boundaries could be dependent on grain size, and we can easily obtain the required defect distribution for dislocation emissions from grain boundaries as the grain size becomes small.

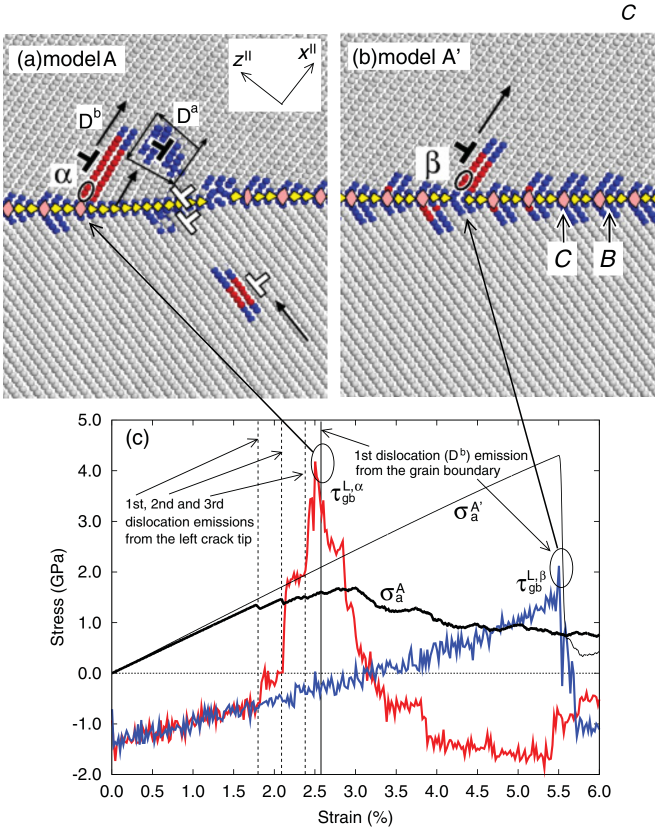

FIG. 8. (Color online) Dislocation emission from a $\Sigma 15$ grain boundary in (a) model A and (b) model A′. (c) Stress-strain curves of models A and A′ under tensile loading.

E. Disclination dipole at grain boundaries

The reason why dislocation D^{a} remains in the vicinity of the grain boundary shown in Fig. 8(a) is investigated by considering the stress fields around nonequilibrium grain boundaries. Figure 9(a) shows the distribution of resolved shear stress $\tau_{z^{\mathrm{II}}x^{\mathrm{II}}}$ just before the dislocation D^{a} emission from the grain boundary containing two lattice dislocations in model A. It should be noted that the atomic configuration is the minimum energy state obtained by the conjugate gradient method to remove thermal vibration effects, and the resolved shear stress field

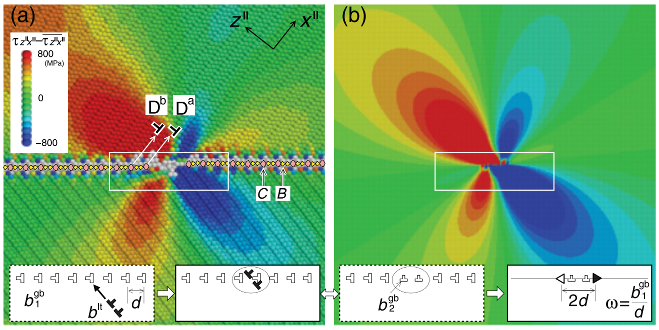

FIG. 9. (Color online) (a) Resolved shear stress field $\tau_{z^{\mathrm{II}}x^{\mathrm{II}}}$ subtracted from the average shear stress field $\overline{\tau_{z^{\mathrm{II}}x^{\mathrm{II}}}}$ when a dislocation D^{a} is ready to be emitted from the grain boundary. The grain boundary contains two lattice dislocations emitted from the left crack tip. (b) Resolved shear stress field $\tau_{z^{\mathrm{II}}x^{\mathrm{II}}}$ by linear elastic theory around the disclination dipole containing two grain-boundary dislocations. The defect configurations correspond to the atomic model as shown in (a).

shown in Fig. 8(a) is subtracted from the average shear stress $\overline{\tau_{z^{\mathrm{II}}x^{\mathrm{II}}}}$ for model A. At the $\Sigma 15$ boundary, C-type structural units at regular intervals d contain grain-boundary dislocations having a component $\boldsymbol{b}_1^{\mathrm{gb}} = \frac{2}{11}[3\bar{1}1]_{\mathrm{I}}$.[35] Here, the subscript I represents the coordinate system of grain I containing a crack. When a lattice dislocation with $\boldsymbol{b}^{\mathrm{lt}} = \frac{1}{2}[\bar{1}10]_{\mathrm{I}}$ is impinged at the $\Sigma 15$ boundary from grain I, the lattice dislocation can react with a grain-boundary dislocation with $\boldsymbol{b}_1^{\mathrm{gb}}$ accompanied by dislocation sliding and climbing along the grain boundary as follows:

$$\boldsymbol{b}_1^{\mathrm{gb}} + \boldsymbol{b}^{\mathrm{lt}} = \frac{1}{22}[174]_{\mathrm{I}} = \boldsymbol{b}_2^{\mathrm{gb}}. \tag{7}$$

As a result, only a grain-boundary dislocation with a parallel component along the grain boundary of $\boldsymbol{b}_2^{\mathrm{gb}} = \frac{1}{22}[174]_{\mathrm{I}}$ (which corresponds to the displacement shift complete lattice[51] of the stable $\Sigma 11$ boundary consisting of only B-type structural units) remains, as shown in the left inset in Fig. 9(b). Based on the lattice defect geometry, the grain-boundary dislocation array expressed by two semi-infinite walls of grain-boundary dislocations with $\boldsymbol{b}_1^{\mathrm{gb}}$ can be represented by a wedge disclination dipole with length $2d$ and the Frank vector $\omega = b_1^{\mathrm{gb}}/d$ as shown in the right inset in Fig. 9(b).[40] Here, d is $5b_2^{\mathrm{gb}}$.[35] Although it could be difficult for crystalline materials to contain disclinations in stable form in the intragranular region, recently disclinations have been recognized as typical defects that can influence the mechanical properties of UFG metals,[52–55] and the stability of disclinations at a grain boundary in bicrystalline nanowires has been studied in computer simulations.[56,57] Figure 9(b) shows the shear stress field of the superposition of each shear stress field $\tau_{z^{\mathrm{II}}x^{\mathrm{II}}}$ of the wedge disclination dipole and two grain-boundary dislocations with $\boldsymbol{b}_2^{\mathrm{gb}}$ calculated using linear elastic theory. The definition of the atomic color is the same as in Fig. 9(a). Although it is difficult to express a dislocation climbing along the grain boundary during the atomic simulations, the stress distributions in the atomic model and those predicted by linear elastic theory are nearly the same. When the applied stress increases further, dislocation $\mathrm{D^a}$ is emitted from the C-type structural unit around the negative disclination shown in Fig. 9(a). However, the stress component $\tau_{z^{\mathrm{II}}x^{\mathrm{II}}}$ ahead of dislocation $\mathrm{D^a}$ does not support the dislocation movement, so dislocation $\mathrm{D^a}$ remains near the grain boundary as shown in Fig. 8(b) where $\tau_{z^{\mathrm{II}}x^{\mathrm{II}}} - \overline{\tau_{z^{\mathrm{II}}x^{\mathrm{II}}}}$ shows negative values. Dislocation $\mathrm{D^a}$ becomes a geometrically necessary dislocation[58] to accommodate the strong elastic field caused by disclinations around the grain boundary. After that, the following dislocation $\mathrm{D^b}$ emitted from the neighbor C-type structural unit of dislocation $\mathrm{D^a}$ can easily move into grain II due to the accommodation of the elastic field by dislocation $\mathrm{D^a}$; finally, the transition of dislocation sources from crack tips to grain boundaries can occur.

As dislocation emissions continue to occur from neighboring C-type structural units shown in Figs. 2(b)–2(d), the $\Sigma 15$ grain-boundary structure transforms into the $\Sigma 11$ boundary structure shown in Fig. 3. Then a wedge disclination dipole with opposite signs is formed at the terminals of the two semi-infinite walls of the grain-boundary dislocations shown in Fig. 3. Generally, disclinations exhibit a long-range stress field, so the stress field could influence the mechanical field around crack tips. In the next section, we investigate the shielding effect caused by disclinations formed at a grain boundary.

F. Disclination shielding

In order to investigate the influence of a disclination dipole near a crack tip on the mechanical field around the crack tip, we introduce a disclination dipole by changing a part of the $\Sigma 15$ boundary into $\Sigma 11$ in model A. The length of a disclination dipole is defined as a_{discli}. A positive disclination is positioned on the active slip plane for dislocations from the left crack tip. The length a_{discli} is increased by moving a negative disclination from the positive disclination because dislocations continue to be emitted from the grain boundary away from the first impinged position shown in Figs. 2(b)–2(d). Figure 10(a) shows the stress field σ_z for grain-boundary shielding for $n_{\mathrm{gb}} = 1$, and Figs. 10(b) and 10(c) shows stress fields of σ_z for the disclination dipole with $a_{\mathrm{discli}} = 3$ nm and 6 nm near the crack tip, respectively, under no applied stress. Although $\sigma_{\mathrm{a}} = 0$, stress fields around the left crack tip with a disclination dipole show negative values in Figs. 10(b) and 10(c), the same as the grain-boundary shielding in Fig. 10(a). Hence, we find that grain boundaries can be equipped with a function of crack-tip shielding caused by a disclination dipole

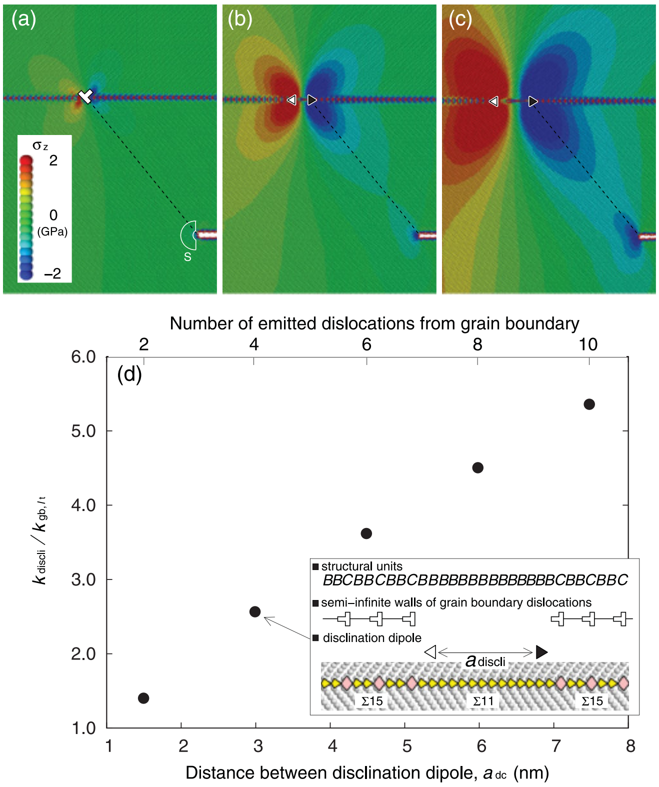

FIG. 10. (Color online) Disclination shielding and its dependence on the distance between the disclination dipole, a_{discli}. Distributions of σ_z by (a) grain-boundary shielding, k_{gb,l_t}, (b) disclination shielding, k_{discli} with $a_{\mathrm{discli}} = 3$ nm and (c) k_{discli} with $a_{\mathrm{discli}} = 6$ nm when the applied stress σ_{a} equals zero. (d) The normalized disclination shielding effect $k_{\mathrm{discli}}/k_{\mathrm{gb},l_t}$ as a function of a_{discli}. The inset figure represents the grain-boundary structure by the combination of structural units B and C, two semi-infinite walls of grain-boundary dislocations, and disclination dipole.

if their structures are partly transformed into other structures by dislocation emissions, and the effect of a disclination dipole on the mechanical field around the crack tip can be called *disclination shielding* or *grain-boundary transformation shielding*. It can be seen that the disclination shielding effect increases with a_{discli} keeping the Frank vector ω by comparison with Figs. 10(b) and 10(c). To further quantify this effect, we compare the average stress values of $\bar{\sigma}_z^{\mathrm{discli}}$ for each a_{discli} and $\bar{\sigma}_z^{\mathrm{gb}}$ for grain-boundary shielding in the region S within a radius of 3 nm as shown in Fig. 10(a). We show the relationship between $\bar{\sigma}_z^{\mathrm{discli}}/\bar{\sigma}_z^{\mathrm{gb}}$ and a_{discli} in Fig. 10(d). Here, we suppose that the values of $\bar{\sigma}_z^{\mathrm{discli}}/\bar{\sigma}_z^{\mathrm{gb}}$ can be regarded as the normalized stress intensity factor for disclination shielding k_{discli} by k_{gb,l_t} for grain-boundary shielding. It can clearly be seen that the stress intensity factor k_{discli} caused by a disclination dipole increases linearly with a_{discli} in Fig. 10(d), and hence, the disclination shielding effect increases as dislocation emissions from grain boundaries occur. Thus, taking disclination shielding into account, the local stress intensity factor k shown in Fig. 6(c) can be expressed as follows:

$$k = K + \sum_{i}^{n_{\mathrm{dislo}}} k_{\mathrm{dislo},i} + \sum_{i}^{n_{\mathrm{gb}}} k_{\mathrm{gb},i} + k_{\mathrm{discli}}. \tag{8}$$

Here, the second term for dislocation shielding contains the effects of dislocations emitted from grain boundaries.

In order to confirm the disclination effect in our atomic simulations, Fig. 11 shows changes in the local tensile stress of $\sigma_{\mathrm{ck}}^{\mathrm{L}} (= \sigma_z)$ at a distance of 0.4 nm from the left crack tip in model A and model B. It should be noted that $\sigma_{\mathrm{ck}}^{\mathrm{L}}$ is normalized by σ_{a} to evaluate the stress concentration of the crack tip, and $\sigma_{\mathrm{ck}}^{\mathrm{L}}/\sigma_{\mathrm{a}}$ is also normalized by $\sigma_{\mathrm{ck}}^{\mathrm{L}}/\sigma_{\mathrm{a}}|_{\varepsilon=0.015}$, representing a state before the first dislocation emission from the crack tip to compare model A with model B. Normalized values of $\sigma_{\mathrm{ck}}^{\mathrm{L}}/\sigma_{\mathrm{a}}$ of model A and model B show nearly the same change with strain and we see a decrease in the stress concentration at the left crack tip caused by the dislocation and grain-boundary shielding effects until dislocation emissions from the grain boundary occur in model A. After dislocation emissions from grain boundaries in model A, the normalized value of $\sigma_{\mathrm{ck}}^{\mathrm{L}}/\sigma_{\mathrm{a}}$ for model A is less than the value of model B shown in Fig. 11. This decrease might be due to the disclination shielding effect caused by the formation of a disclination dipole at the grain boundaries where dislocations have already been emitted.

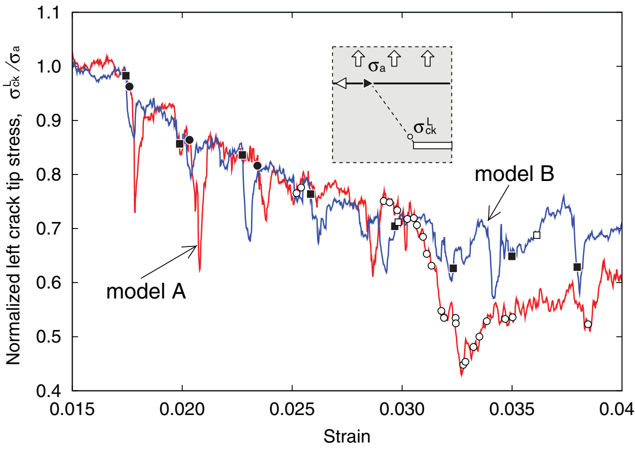

FIG. 11. (Color online) Normalized left crack tip stress $\sigma_{\mathrm{ck}}^{\mathrm{L}}/\sigma_{\mathrm{a}}$ at a distance of 0.4 nm from the left crack tip. The values of $\sigma_{\mathrm{ck}}^{\mathrm{L}}/\sigma_{\mathrm{a}}$ are also normalized by the values $\sigma_{\mathrm{ck}}^{\mathrm{L}}/\sigma_{\mathrm{a}}|_{\varepsilon=0.015}$ when $\varepsilon = 0.015$ in order to compare values between model A and model B. Solid and open marks represent dislocation emissions from the left crack tip and the upper-left grain boundary, respectively.

IV. DISCUSSION

Based on the results obtained in our atomic-scale computational experiments, we can now propose a mechanism for improving the fracture toughness in UFG metals as follows. At the beginning of the deformation, a crack tip act as the main dislocation source and can generate many dislocations. After that, the dislocation and grain-boundary shielding effects caused by dislocations emitted from the crack tip can improve the fracture toughness K_{IC} to be greater than K_{gf}. However, the stress intensity factor K_{e} required for dislocation emission from the crack tip also increases with the number of dislocations around the crack tip, and then it becomes difficult to make further emission of dislocations from the crack tip. Therefore, the local stress intensity factor k immediately reaches K_{gf}, and then the crack extension occurs in a brittle manner. Since the grain-boundary shielding effect is dependent on grain size in general, K_{IC} should become small as the grain size becomes small. On the other hand, when grain boundaries also act as a dislocation source, a switching of dominant dislocation sources from crack tips to grain boundaries occurs by two transitions due to the dislocation pileup against grain boundaries and impinging dislocations at grain boundaries. One transition is a shift of the highly concentrated stress field from crack tips to grain boundaries, and the other is a structural change from a stable grain-boundary structure to an unstable grain-boundary structure containing EGBDs. After dislocation emissions from unstable grain boundaries accompanied by transformation of grain-boundary structure with long periodicity into the neighboring favored boundary, a disclination dipole can be formed at grain boundaries. When emitted dislocations from grain boundaries have the character of an antishielding effect on the crack tip, the disclination dipole necessarily induces shielding effect on the crack tip. Figure 12 shows the local stress intensity factor $k_{\mathrm{dislo},i}$ map for emitted dislocation i from the grain boundary calculated by Eq. (16.7) in Ref. 41, which is the general expression of Eq. (2). We can see that all emitted dislocations gliding into grain I or grain II have an antishielding effect on the crack tip. In order to release the elastic strain energy to suppress the crack extension in a brittle manner, the emitted dislocations should glide away from the grain boundary where they are generated and also from the crack tip. Hence, we can expect that the grain boundary containing the disclination dipole can be equipped with a function of crack-tip shielding when those emitted antishielding dislocations glide a long distance.

The obvious difference between the dislocation shielding and the disclination shielding is whether relative positions between the crack tip and these lattice defects causing the (anti)shielding effect change or not under applied loading. Hence, we can presume that the more antishielding

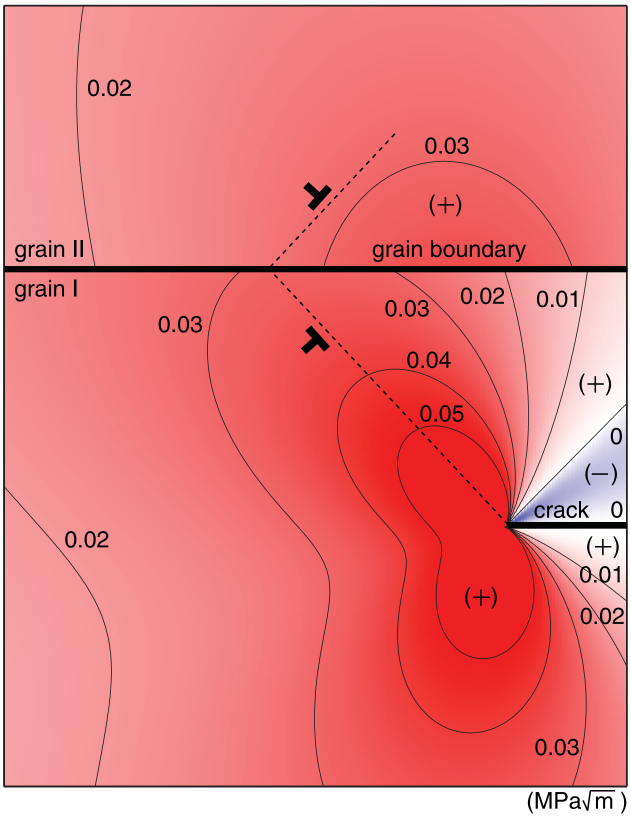

FIG. 12. (Color online) Local stress intensity factor $k_{\mathrm{dislo},i}$ map for emitted dislocation i from the grain boundary.

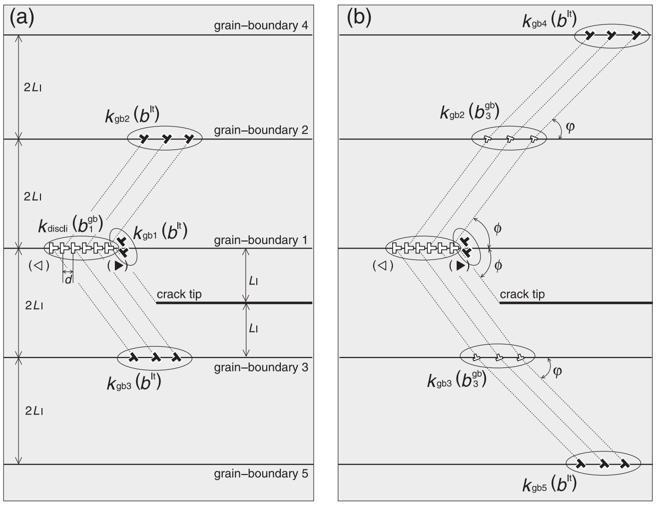

FIG. 13. Dislocation distributions around the crack tip. All dislocations are at grain boundaries. Total Burgers vectors in (a) and (b) are the same, but internal stress distributions around the crack tip are different. These pictures correspond to the states after six dislocations are emitted from grain boundary 1.

dislocations glide away from grain boundaries where they are generated, the stronger the disclination shielding effect becomes. In order to investigate the influence of internal stress redistribution due to antishielding dislocation glides on the local stress intensity factor k, we estimate k for two situations in the multilayer aluminum containing a crack and two EGBDs emitted from the crack tip shown in Fig. 13 by Eq. (16.7) in Ref. 41. L_{I}, d, b^{lt}, b_1^{gb}, b_2^{gb}, ϕ, and the structure of grain boundary 1 are the same in model A. The first situation shown in Fig. 13(a) is that all antishielding dislocations emitted from grain boundary 1 impinge on grain boundaries 2 and 3; hence $k_{\mathrm{total}}^{(1)}$ can be calculated as the sum of k_{gb1} caused by two EGBDs impinging from the crack tip, k_{gb2} and k_{gb3} caused by the antishielding lattice dislocations at grain boundaries 2 and 3, and k_{discli} caused by the finite array of grain-boundary dislocations with b_1^{gb}. The second situation shown in Fig. 13(b) is that the emitted antishielding dislocations from grain boundary 1 can transit across grain boundaries 2 and 3 leaving residual grain-boundary dislocations with b_3^{gb} at grain boundary 2 and 3, and impinge on grain boundaries 4 and 5. Hence, $k_{\mathrm{total}}^{(2)}$ can be calculated as the sum of k_{gb1}, k_{gb2}, and k_{gb3} caused by the residual grain-boundary dislocations with b_3^{gb} at grain boundaries 2 and 3, k_{gb4} and k_{gb5} caused by the lattice dislocations at grain boundaries 4 and 5, and k_{discli}. Since φ is set to 45° in order to obtain the maximum Schmid factor, the magnitude of Burgers vector b_3^{gb} of residual grain-boundary dislocations at grain boundaries 4 and 5 is approximately $0.1b^{\mathrm{lt}}$. Figure 14 shows each local stress intensity factor k_{gb} and k_{discli} and total local stress intensity factor k_{total} for two situations. In order to avoid consideration of grain-boundary dislocation effect with b_2^{gb} at grain boundary 1 generated by an antishielding dislocation emission from the C-type structural unit in grain boundary 1, k is calculated for every two dislocation emissions from grain boundary 1. In both situations, k_{gb1} and k_{discli} take the same values, and the shielding effect caused by the disclination dipole increases as antishielding dislocation emissions from grain boundary 1 occur. For situation 1, the antishielding effect caused by emitted dislocations from grain boundary 1 at grain boundaries 2 and 3 also increases with the number of emitted dislocations from grain boundary 1. Therefore, although total local stress intensity factor $k_{\mathrm{total}}^{(1)}$ shows shielding effect, $k_{\mathrm{total}}^{(1)}$ shows a nearly constant value even though the number of emitted dislocations from grain boundary 1 increases. On the other hand, for situation 2, the antishielding effect caused by $k_{\mathrm{gb2}} \sim k_{\mathrm{gb5}}$ is smaller than k_{gb2} and k_{gb3} of situation 1 because of the expansion of the plastic deformation zone by the antishielding dislocation movement. However, the disclination dipole at grain boundary 1 does not move away from the crack tip. Hence, the absolute value of the total local stress intensity factor $k_{\mathrm{total}}^{(2)}$ increases as the number of emitted dislocations from grain boundary 1 increases.

Finally, disclination shielding could decrease k without further dislocation emissions from the crack tip, and the effect can improve the fracture toughness in UFG metals. Furthermore, dislocation sources are switched from crack tips to grain boundaries, and the density of mobile dislocations increases dramatically. Therefore, the tendency for plastic deformation around the crack tip is also improved even at low temperatures, as compared to the case where grain boundaries do not emit dislocations at all. This mechanism to increase the mobile dislocation density by dislocation emission from grain boundaries implies a decrease of the DBTT with grain

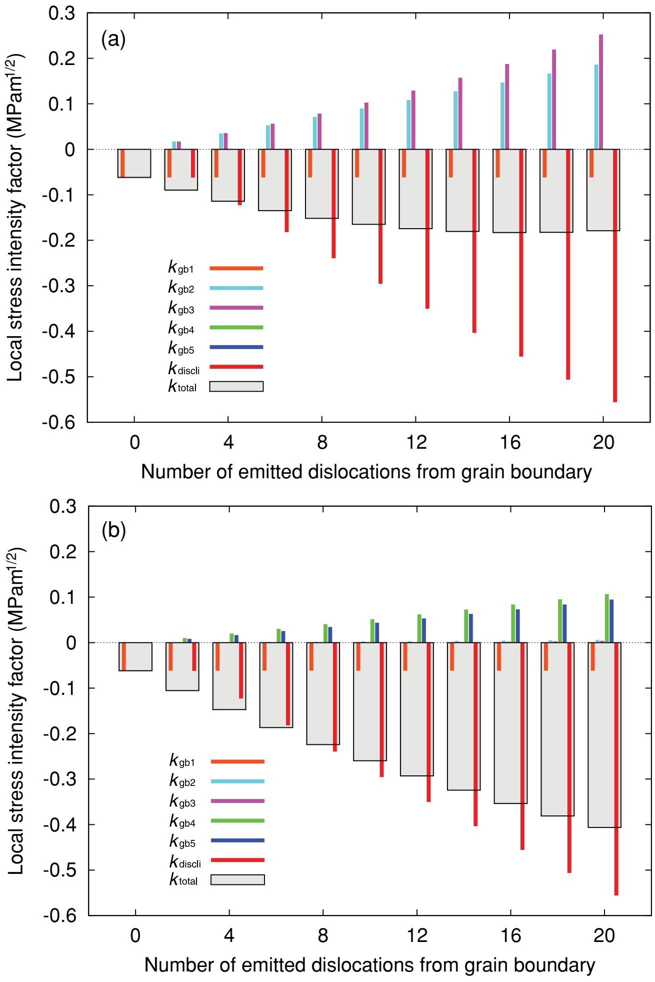

FIG. 14. (Color online) Local stress intensity factors for (a) situation 1 and (b) situation 2. $k_{\text{total}} = k_{\text{gb1}} + k_{\text{gb2}} + k_{\text{gb3}} + k_{\text{gb4}} + k_{\text{gb5}} + k_{\text{discli}}$.

refinement. Thus, in fracture phenomena of UFG metals, it is very important to consider the roles of grain boundaries, not only as obstacles against dislocation movement, but also as dislocation sources. Fracture toughness of UFG metals can be considered based on the internal stress redistribution caused by the interaction between mobile lattice dislocations and stable grain-boundary dislocations.

V. CONCLUSIONS

In order to investigate the roles of grain boundaries in improving the fracture toughness of UFG metals, as reported in actual experiments, we perform interaction simulations of crack tips, dislocations, and grain boundaries in aluminum bicrystal models using molecular dynamics. Based on the results of our atomic simulations, the role of grain boundaries as dislocation sources should be essential to elucidate fracture phenomena in UFG metals, because grain boundaries that only function as obstacles to dislocation movement make materials brittle by dislocation and grain-boundary shielding effects as the grain size becomes small. A proposed mechanism to express the improved fracture toughness in UFG metals is the disclination shielding effect on the crack tip mechanical field. Disclination shielding can be activated when a transition of dislocation sources from crack tips to grain boundaries occurs, and the effect becomes pronounced as anti-shielding dislocations are continuously emitted from grain boundaries without dislocation emissions from crack tips. This mechanism can shield the mechanical field around the crack tip and obtain plastic deformation by dislocation emissions from grain boundaries; hence it can be expected that the disclination shielding effect can improve the fracture toughness in UFG metals. The proposed mechanism is constructed on the basis of our atomic simulation results, but the deformation conditions, e.g., strain rate, are far from the actual experimental ones. Therefore, we will try to further inspect the possibility of the proposed disclination shielding at grain boundaries by the free-end nudged elastic band method;[59,60] we will also attempt the direct measurement of displacement field around grain boundaries near a crack tip by high-resolution electron microscopy[61,62] and study three-dimensional dislocation configurations around grain boundaries by electron tomography[63] in actual UFG metals.

ACKNOWLEDGMENTS

The authors would like to thank N. Tsuji and H. Nakashima for fruitful discussions. T.S. acknowledges support from the Ministry of Education, Science, Sports, and Culture, Grant-in-Aid for Young Scientists (B), 2009, 19760061. This study was financially supported by a Grant-in-Aid for Scientific Research on Innovative Area, Bulk Nanostructured Metals, through MEXT, Japan (Contracts No. 22102006 and No. 22102007), and the support is gratefully appreciated.

---

[1] E. O. Hall, Proc. Phys. Soc. B **64**, 747 (1951).
[2] N. J. Petch, J. Iron Steel Inst. **174**, 25 (1953).
[3] A. H. Chokshi, A. Rosen, J. Karch, and H. Gleiter, Scr. Metall. **23**, 1679 (1989).
[4] G. E. Fougere, J. R. Weertman, R. W. Siegel, and S. Kim, Scr. Metall. Mater. **26**, 1879 (1992).
[5] P. G. Sanders, J. A. Eastman, and J. R. Weertman, Acta Mater. **45**, 4019 (1997).
[6] R. A. Masumura, P. M. Hazzledine, and C. S. Pande, Acta Mater. **46**, 4527 (1998).
[7] A. S. Khan, H. Zhang, and L. Takacs, Int. J. Plasticity **16**, 1459 (2000).
[8] J. Schiøtz, T. Vegge, F. D. Di Tolla, and K. W. Jacobsen, Nature (London) **391**, 561 (1998).
[9] V. Yamakov, D. Wolf, S. R. Phillpot, A. K. Mukherjee, and H. Gleiter, Philos. Mag. Lett. **83**, 385 (2003).
[10] J. Schiøtz and K. W. Jacobsen, Science **301**, 1357 (2003).
[11] T. Shimokawa, A. Nakatani, and H. Kitagawa, Phys. Rev. B **71**, 224110 (2005).

[12] J. M. Hodge, R. D. Manning, and H. M. Reichhold, Trans. Am. Inst. Min. Metall. Eng. **185**, 233 (1949).

[13] Y. Iwahashi, Z. Horita, M. Nemoto, J. Wang, and T. G. Langdon, Scr. Mater. **35**, 143 (1996).

[14] Y. Saito, H. Utsunomiya, N. Tsujia, and T. Sakaia, Acta. Mater. **47**, 579 (1999).

[15] R. Z. Valiev, Y. V. Ivanisenko, E. F. Rauch, and B. Baudelet, Acta. Mater. **44**, 4705 (1996).

[16] N. Tsuji, S. Okuno, Y. Koizumi, and Y. Minamino, Mater. Trans. **45**, 2272 (2004).

[17] M. Tanaka, N. Fujimoto, and K. Higashida, Mater. Trans. **49**, 58 (2008).

[18] M. Tanaka, K. Higashida, T. Shimokawa, and T. Morikawa, Mater. Trans. **50**, 56 (2009).

[19] J. R. Rice and R. Thomson, Philos. Mag. **29**, 73 (1974).

[20] B. S. Majumdar and S. J. Burns, Acta Metall. **29**, 579 (1981).

[21] K. Higashida, M. Tanaka, A. Hartmaier, and Y. Hoshino, Mater. Sci. Eng. A **483-484**, 13 (2008).

[22] S. Fujita, K. Maeda, and S. Hyodo, Philos. Mag. A **65**, 131 (1992).

[23] P. B. Hirsch, A. S. Booth, M. Ellis, and S. G. Roberts, Scr. Mater. **27**, 1723 (1992).

[24] A. Hartmaier and P. Gumbsch, Phys. Rev. B **71**, 024108 (2005).

[25] J. Dana Honeycutt and H. C. Andersen, J. Phys. Chem. **91**, 4950 (1987).

[26] S. J. Noronha and D. Farkas, Mater. Sci. Eng. A **365**, 156 (2004).

[27] X. Zeng and A. Hartmaier, Acta Mater. **58**, 301 (2010).

[28] L. Murr, Mater. Sci. Eng. **51**, 71 (1981).

[29] T. C. Lee, I. M. Robertson, and H. K. Birnbaum, Metall. Trans. A **21**, 2437 (1990).

[30] A. Frøseth, P. Derlet, and H. Van Swygenhoven, Acta Mater. **52**, 5863 (2004).

[31] D. E. Spearot, M. A. Tschopp, K. I. Jacob, and D. L. McDowell, Acta Mater. **55**, 705 (2007).

[32] M. Tschopp, G. Tucker, and D. McDowell, Acta Mater. **55**, 3959 (2007).

[33] T. Shimokawa, T. Kinari, and S. Shintaku, Phys. Rev. B **75**, 144108 (2007).

[34] M. Tschopp, G. Tucker, and D. McDowell, Comput. Mater. Sci. **44**, 351 (2008).

[35] T. Shimokawa, Phys. Rev. B **82**, 174122 (2010).

[36] Y. Mishin, D. Farkas, M. J. Mehl, and D. A. Papaconstantopoulos, Phys. Rev. B **59**, 3393 (1999).

[37] M. P. Allen and D. J. Tildesley, *Computer Simulation of Liquids* (Oxford University Press, New York, 1987).

[38] M. Parrinello and A. Rahman, Phys. Rev. Lett. **45**, 1196 (1980).

[39] See Supplemental Material at http://link.aps.org/supplemental/10.1103/PhysRevB.83.214113 for the movie of a transition of dislocation sources from the crack tip to the grain boundary.

[40] A. E. Romanov and V. I. Vladimirov, ed., *Disclinations in Crystalline Solids,* in *Dislocations in Solids*, edited by F. R. N. Nabarro, Vol. 9 (North Holland, Amsterdam, 1992).

[41] R. Thomson, *Solid State Physics*, Vol. 39 (Academic, New York, 1986), p. 1.

[42] K. Higashida and N. Narita, *Lattice Defects in Ceramics*, JJAP Series (McGraw-Hill, 1989).

[43] W. Voigt, *Lehrbuch der Kristallphysik* (Teubner, Leipzig, 1928).

[44] J. Weertman, *Dislocation Based Fracture Mechanics* (World Scientific, Singapore, 1996).

[45] Y. Murakami, *Stress Intensity Factor Handbook*, Vols. 1 and 2 (Pergamon, Oxford, 1987).

[46] J. P. Hirth and J. Lothe, *Theory of Dislocations*, 2nd ed. (McGraw-Hill, New York, 1968).

[47] L. Priester, Interface Sci. **4**, 205 (1997).

[48] B. Décamps, L. Priester, and J. Thibault, Adv. Eng. Mater. **6**, 814 (2004).

[49] G. Richter, K. Hillerich, D. S. Gianola, R. Mönig, O. Kraft, and C. A. Volkert, Nano Lett. **9**, 3048 (2009).

[50] A. A. Griffith, Philos. Trans. R. Soc. London A **221**, 163 (1921).

[51] W. Bollmann, *Crystal Defects and Crystalline Interfaces* (Springer, 1970).

[52] R. Z. Valiev, R. K. Islamgaliev, and I. V. Alexandrov, Prog. Mater. Sci. **45**, 103 (2000).

[53] M. Murayama, J. M. Howe, H. Hidaka, and S. Takaki, Science **295**, 2433 (2002).

[54] I. A. Ovid'ko, Science **295**, 2386 (2002).

[55] I. A. Ovid'ko and A. G. Sheinerman, Phys. Rev. B **77**, 054109 (2008).

[56] K. Zhou, A. A. Nazarov, and M. S. Wu, Phys. Rev. B **73**, 045410 (2006).

[57] K. Zhou, A. A. Nazarov, and M. S. Wu, Phys. Rev. Lett. **98**, 035501 (2007).

[58] M. F. Ashby, Philos. Mag. **21**, 399 (1970).

[59] T. Zhu, J. Li, A. Samanta, H. G. Kim, and S. Suresh, Proc. Natl. Acad. Sci. USA **104**, 3031 (2007).

[60] T. Zhu, J. Li, A. Samanta, A. Leach, and K. Gall, Phys. Rev. Lett. **100**, 025502 (2008).

[61] M. J. Hÿtch, J. L. Putaux, and J. M. Pénisson, Nature (London) **423**, 270 (2003).

[62] C. L. Johnson, M. J. Hÿtch, and P. R. Buseck, Proc. Natl. Acad. Sci. USA **101**, 17936 (2004).

[63] M. Tanaka, K. Higashida, K. Kaneko, S. Hata, and M. Mitsuhara, Scr. Mater. **59**, 901 (2008).